Concomitant Length and Diameter Separation of Single-Walled Carbon Nanotubes

Daniel A. Heller,[†] Rebecca M. Mayrhofer,[‡] Seunghyun Baik,[‡,⊥] Yelena V. Grinkova,[§] Monica L. Usrey,[‡] and Michael S. Strano*,[‡]

Contribution from the Departments of Chemistry, Chemical and Biomolecular Engineering, and Biochemistry, University of Illinois at Urbana–Champaign, Urbana, Illinois 61801

Received June 16, 2004; E-mail: strano@uiuc.edu

Abstract: Gel electrophoresis and column chromatography conducted on individually dispersed, ultrasonicated single-walled carbon nanotubes yield simultaneous separation by tube length and diameter. Electroelution after electrophoresis is shown to produce highly resolved fractions of nanotubes with average lengths between 92 and 435 nm. Separation by diameter is concomitant with length fractionation, and nanotubes that have been cut shortest also possess the greatest relative enrichments of large-diameter species. Longer sonication time causes increased electrophoretic mobility in the gels; thus, ultrasonic processing determines the degree of both length and diameter separation of the nanotubes. The relative quantum yield decreases nonlinearly as the nanotube length becomes shorter. These techniques constitute a preparative, scalable method for separating nanotubes by two important attributes required for electronic and sensor applications.

Introduction

Important advances in single-walled carbon nanotube (SWNT) separation[1–9] are necessary for future development of nanotube-based technologies. Further advances in electronic,[10–12] structural,[13–15] and sensor[16,17] applications will be dependent on the ability to exert precise control over the SWNT diameter,[6–8] length,[1–5,9] and electronic structure.[12,18,19]

Nanotubes can be classified by two integers (*n,m*) which define their diameter and electronic structure.[20] By conceptually rolling and connecting point (0,0) with point (*n,m*) on a graphene coordinate plane, all possible nanotube diameters and geometries can be formed.[21] Raman spectroscopy, used to identify particular (*n,m*) nanotubes within a sample, is employed to benchmark separation processes.[22] The Raman radial breathing modes (RBMs), in the low-wavenumber region of the Raman spectrum, correspond to axial vibrations of nanotubes in the sample whose frequencies are in resonance with the excitation laser. The Raman shifts of nanotube RBMs are inversely proportional to the SWNT diameter.[23,24]

The electronic structure and diameter of carbon nanotubes determine the electronic transitions probed via absorption and fluorescence spectroscopies.[24] Due to the quasi 1-D structure of nanotubes, diameter-dependent van Hove maxima appear in the density of states. This causes absorption spectra of SWNTs to display sharp interband transitions associated with van Hove singularities E_{11} (v1 → c1), E_{22}, and E_{33} of semiconducting and

[†] Department of Chemistry.
[‡] Department of Chemical and Biomolecular Engineering.
[§] Department of Biochemistry.
[⊥] School of Mechanical Engineering, Sungkyunkwan University, Suwon 440-746, South Korea.
(1) Doorn, S. K.; Fields, R. E.; Hu, H.; Hamon, M. A.; Haddon, R. C.; Selegue, J. P.; Majidi, V. *J. Am. Chem. Soc.* **2002**, *124*, 3169−3174.
(2) Doorn, S. K.; Strano, M. S.; O'Connell, M. J.; Haroz, E. H.; Rialon, K. L.; Hauge, R. H.; Smalley, R. E. *J. Phys. Chem. B* **2003**, *107*, 6063−6069.
(3) Duesberg, G. S.; Blau, W.; Byrne, H. J.; Muster, J.; Burghard, M.; Roth, S. *Synth. Met.* **1999**, *103*, 2484−2485.
(4) Duesberg, G. S.; Muster, J.; Krstic, V.; Burghard, M.; Roth, S. *Appl. Phys. A: Mater. Sci. Process.* **1998**, *67*, 117−119.
(5) Farkas, E.; Anderson, M. E.; Chen, Z. H.; Rinzler, A. G. *Chem. Phys. Lett.* **2002**, *363*, 111−116.
(6) Strano, M. S.; Zheng, M.; Jagota, A.; Onoa, G. B.; Heller, D. A.; Barone, P. W.; Usrey, M. L. *Nano Lett.* **2004**, *4*, 543−550.
(7) Zheng, M.; Jagota, A.; Semke, E. D.; Diner, B. A.; Mclean, R. S.; Lustig, S. R.; Richardson, R. E.; Tassi, N. G. *Nat. Mater.* **2003**, *2*, 338−342.
(8) Zheng, M.; Jagota, A.; Strano, M. S.; Santos, A. P.; Barone, P.; Chou, S. G.; Diner, B. A.; Dresselhaus, M. S.; McLean, R. S.; Onoa, G. B.; Samsonidze, G. G.; Semke, E. D.; Usrey, M.; Walls, D. J. *Science* **2003**, *302*, 1545−1548.
(9) O'Connell, M. J.; Boul, P.; Ericson, L. M.; Huffman, C.; Wang, Y. H.; Haroz, E.; Kuper, C.; Tour, J.; Ausman, K. D.; Smalley, R. E. *Chem. Phys. Lett.* **2001**, *342*, 265−271.
(10) Avouris, P. *Chem. Phys.* **2002**, *281*, 429−445.
(11) Avouris, P.; Martel, R.; Derycke, V.; Appenzeller, J. *Physica B* **2002**, *323*, 6−14.
(12) Heinze, S.; Tersoff, J.; Martel, R.; Derycke, V.; Appenzeller, J.; Avouris, P. *Phys. Rev. Lett.* **2002**, *89*, 106801.
(13) Thostenson, E. T.; Ren, Z. F.; Chou, T. W. *Compos. Sci. Technol.* **2001**, *61*, 1899−1912.
(14) Roche, S. *Ann. Chim. (Paris)* **2000**, *25*, 529−532.
(15) Clarke, A. C. *Sci. Am.* **2001**, *284*, 11−11.
(16) Wohlstadter, J. N.; Wilbur, J. L.; Sigal, G. B.; Biebuyck, H. A.; Billadeau, M. A.; Dong, L. W.; Fischer, A. B.; Gudibande, S. R.; Jamieson, S. H.; Kenten, J. H.; Leginus, J.; Leland, J. K.; Massey, R. J.; Wohlstadter, S. J. *Adv. Mater.* **2003**, *15*, 1184−1187.
(17) Chen, R. J.; Choi, H. C.; Bangsaruntip, S.; Yenilmez, E.; Tang, X. W.; Wang, Q.; Chang, Y. L.; Dai, H. J. *J. Am. Chem. Soc.* **2004**, *126*, 1563−1568.
(18) Avouris, P. *Acc. Chem. Res.* **2002**, *35*, 1026−1034.
(19) Strano, M. S.; Dyke, C. A.; Usrey, M. L.; Barone, P. W.; Allen, M. J.; Shan, H. W.; Kittrell, C.; Hauge, R. H.; Tour, J. M.; Smalley, R. E. *Science* **2003**, *301*, 1519−1522.
(20) Strano, M. S.; Doorn, S. K.; Haroz, E. H.; Kittrell, C.; Hauge, R. H.; Smalley, R. E. *Nano Lett.* **2003**, *3*, 1091−1096.
(21) Saito, R.; Dresselhaus, G.; Dresselhaus, M. S. *Physical Properties of Carbon Nanotubes*; Imperial College Press: London, 1998.
(22) Moore, V. C.; Strano, M. S.; Haroz, E. H.; Hauge, R. H.; Smalley, R. E.; Schmidt, J.; Talmon, Y. *Nano Lett.* **2003**, *3*, 1379−1382.
(23) Strano, M. S. *J. Am. Chem. Soc.* **2003**, *125*, 16148−16153.
(24) Doorn, S. K.; Heller, D. A.; Barone, P. W.; Usrey, M. L.; Strano, M. S. *Appl. Phys. A: Mater. Sci. Process.* **2004**, *78*, 1147−1155.

metallic nanotubes. Semiconducting nanotubes also display near-infrared fluorescence features in the 800−1600 nm range consistent with first van Hove (E_{11}) transitions.[25,26] Although nanotube lengths cannot thus far be determined via spectroscopy, the aforementioned techniques are rich in SWNT diameter and electronic structure information.
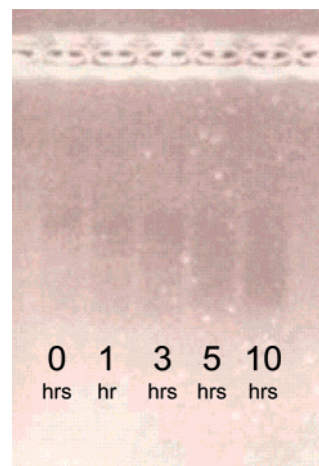
Significant advances in length[1−5,9] and diameter[6−8] separation of nanotubes have been made over the past few years. The most advanced separation work has been completed by Zheng and co-workers[7,8] using a DNA wrapping procedure followed by ion exchange chromatography to yield nanotubes separated into fractions of narrow species distribution. The basis of separation appears to be primarily by diameter, although some electronic component may also be operative.[6] This technique may prove difficult to scale, however, because of the precise sequence of DNA needed for separation.

Length separation of nanotubes has been carried out using various chromatographic techniques.[1−5,9] Size exclusion chromatography of raw SWNT material has produced fractions of individual and bundled nanotubes with mean lengths around 200 nm.[4,5] Capillary electrophoresis (CE) produces length-separated fractions, the shortest consisting of nanotubes averaging less than 250 nm.[1,2] To enhance length separation, SWNT cutting has been achieved using nitric acid to shorten nanotubes from the ends.[5] This method also causes significant functionalization and damage of the nanotube sidewall, however, which perturbs the electronic structure.[27]

In this study, we demonstrate a scalable method for generating length- and diameter-separated carbon nanotubes via ultrasonication and chromatography. Material is characterized by atomic force microscopy (AFM) and Raman, fluorescence, and absorption spectroscopies. The cutting process in our system is found to be diameter-selective, causing length fractions to exhibit enrichment or depletion of nanotubes of certain widths. Specifically, we find that shorter nanotubes are enriched in large-diameter species, while longer nanotube fractions are enriched with small-diameter tubes.

Experimental Section

Single-walled carbon nanotubes produced by the HiPco method[28] were obtained from Rice University. Nanotubes were suspended in 100 mM sodium cholate hydrate (Sigma) by cup-horn sonication for 10 min and centrifugation for 4 h at 30000 rpm.[25] The supernatant was retained and sonicated for 1−10 h at 3 W using a probe-tip sonicator (Vibra Cell) in a cooling cell apparatus (Vibra Cell). Electrophoresis was performed in a 7 × 10 cm, 1% agarose gel in TAE buffer (Tris−acetate−EDTA) with 50 mM sodium cholate at 100 V. Nanotube fractions were removed from the gel via electroelution by creating a second set of eight wells in the gel 4.5 cm from the original 40 μL sample wells. Material was pipetted out of the second set of wells after 30 min of electrophoresis and repeatedly after an additional 5 min of applied potential to obtain six fractions. Gravity flow size exclusion chromatography was performed with Sephacryl S-500 gel filtration chromatography medium (Amersham Biosciences) in a 100 cm Kontes

(25) O'Connell, M. J.; Bachilo, S. M.; Huffman, C. B.; Moore, V. C.; Strano, M. S.; Haroz, E. H.; Rialon, K. L.; Boul, P. J.; Noon, W. H.; Kittrell, C.; Ma, J. P.; Hauge, R. H.; Weisman, R. B.; Smalley, R. E. *Science* **2002**, *297*, 593−596.
(26) Saito, R.; Dressenhaus, G.; Dresselhaus, M. S. *Physical Properties of Carbon Nanotubes*; Imperial College Press: London, 1998.
(27) Strano, M. S.; Huffman, C. B.; Moore, V. C.; O'Connell, M. J.; Haroz, E. H.; Hubbard, J.; Miller, M.; Rialon, K.; Kittrell, C.; Ramesh, S.; Hauge, R. H.; Smalley, R. E. *J. Phys. Chem. B* **2003**, *107*, 6979−6985.
(28) Bronikowski, M. J.; Willis, P. A.; Colbert, D. T.; Smith, K. A.; Smalley, R. E. *J. Vac. Sci. Technol., A* **2001**, *19*, 1800−1805.

Figure 1. Agarose gel run for 30 min containing nanotubes probe-tip sonicated for various durations. The material in the lane labeled "0 hrs" was cup-horn sonicated for 10 min with no further probe-tip sonication. The other lanes contain solutions similarly cup-horn sonicated and additionally probe-tip sonicated for 1, 3, 5, and 10 h.
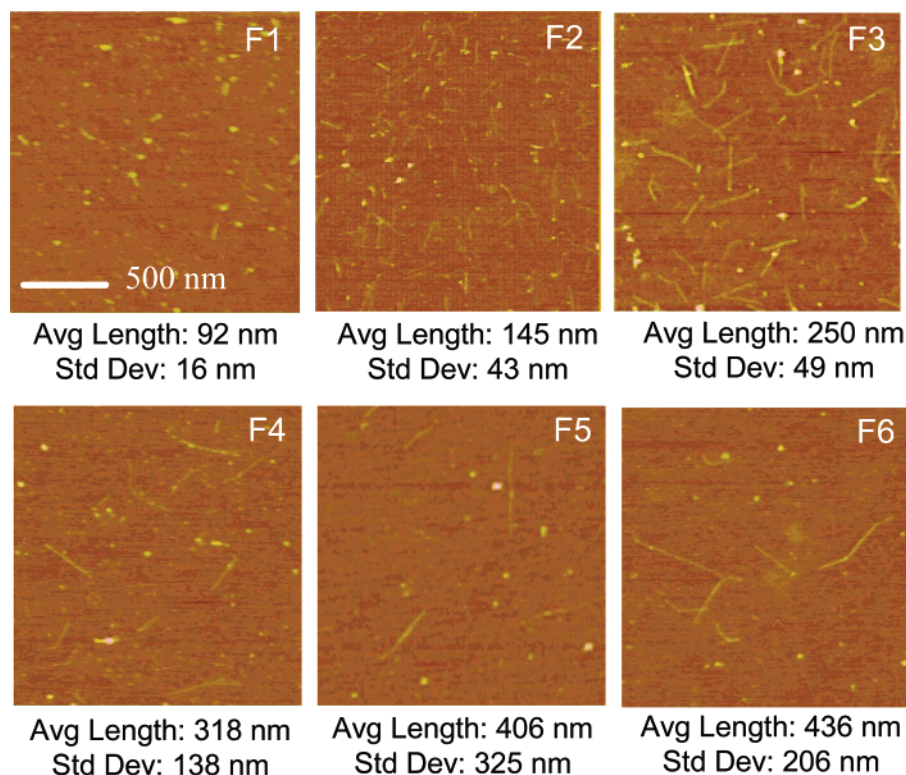
FlexColumn economy column (Fischer) with a 1.5 cm internal diameter using TAE buffer with 50 mM sodium cholate.

Raman spectroscopy at 633 nm excitation was performed with a LabRam-IR (Jobin Yvon Horiba) and at 785 nm using a Kaiser Optical Holospec f/1.8 imaging spectrograph with a fiber optic probe head incorporating both collection optics and excitation laser aperture. The spectrometer also measured fluorescence peaks to approximately 1080 nm. Raman/fluorescence spectra were taken on electrophoresis gels by aiming the probe head 90° into the agarose gel. The gels were held on an automated *x*−*y* translation stage which moved 0.5 mm between every spectrum taken. This produced spatially parsed sets of Raman spectra over the length of the gel. Spectra were processed via the Kaiser Holoreact program for Matlab (The Mathworks, Inc.). Peak heights of all Raman and fluorescence features were calculated at defined wavelength intervals over each spectrum in the gel. A Shimadzu UV-3101PC UV−vis−near-IR scanning spectrophotometer was used for absorption spectra. Fluorescence spectroscopy measurements between 900 and 1400 nm were conducted with a spectrofluorimeter built in-house and a liquid nitrogen-cooled Edinburgh Instruments EI-L Ge detector. AFM samples were prepared by depositing nanotube solutions onto silicon wafers coated with (3-aminopropyl)triethoxysilane (APTES) and rinsed with water. Tapping mode AFM images were taken with a Digital Instruments Dimension 3100 with BS-Tap300Al silicon probes (Budget Sensors).

Results and Discussion

Length Separation. Gel electrophoresis using field strengths of 7 V/cm for 30 min was performed on carbon nanotubes produced by the HiPco process, suspended in water with sodium cholate, and sonicated for five different durations. The SWNT samples, initially cup-horn sonicated for 10 min, and then subsequently probe-tip sonicated for an additional 0, 1, 3, 5, and 10 h, result in different degrees of nanotube migration into the gel (Figure 1). The resulting agarose gel, run in TAE buffer with 50 mM sodium cholate, shows that faster migration results as the probe-tip sonication duration increases. In the control (0 h), material appears closest to the sample wells, with some material failing to migrate out of the well at all. In the lane containing nanotubes probe-tip sonicated for 10 h, material concentrates further from the wells and leaves no residual material in them. The other samples show a systematic increase in migration with sonication time.

Figure 2. Atomic force micrographs of six electroeluted gel fractions of nanotubes sonicated for 10 h. Material is removed from a set of wells placed 4.5 cm from the original sample wells. F1 is the first eluted fraction. Each successive fraction elutes after an additional 5 min of applied potential. Average nanotube lengths and standard deviations are listed for each fraction. All images use the same scale.

AFM measurements of nanotubes electroeluted from a gel run under identical conditions (7 V/cm, 30 min, 10 h of sonication) reveal length-dependent separation (Figure 2). The first fraction of electroeluted material, which moves at the highest velocity from the sample wells, contains nanotubes with an average length of 92 nm. Nanotubes in fraction F2 average 144 nm, while those in F3 average 254 nm. The mean length appearing in fraction 6 is 435 nm, but the standard deviation of lengths increases greatly for the later fractions. We conclude from these measurements that gel electrophoresis separates nanotubes primarily by length, as the shortest nanotubes move most quickly through the gel, and that sonication cuts nanotubes in proportion to the duration of ultrasonic processing.

Diameter Separation. The heights of 20 nanotubes on the silicon substrate were measured from each of fractions 1, 3, and 6 via AFM. The mean heights are 0.829, 0.789, and 0.585 nm with standard deviations of 0.134, 0.201, and 0.146 nm, respectively. These values appear low compared with the range of typical HiPco diameters (0.6–1.2 nm) despite calibration using etched mica and controlling for deformation due to tip compression. Burghard and co-workers suggest that ATPES, used to adhere SWNT to the silicon surface, can mask heights as nanotubes recess within the monolayer.[29] Nevertheless, the trend of relative heights suggests that shorter nanotubes, which move more quickly in the gel, possess larger diameters (by 30%).

Raman and fluorescence data of nanotubes in the gels were measured for the 10 h sonicated sample after voltage was applied for 1 h. Using an automated translation stage, Raman/fluorescence spectra at 785 nm excitation were taken every 0.5 mm from the sample well to the end of the gel lane (Figure 3). Figure 4a presents the normalized intensities of four different Raman
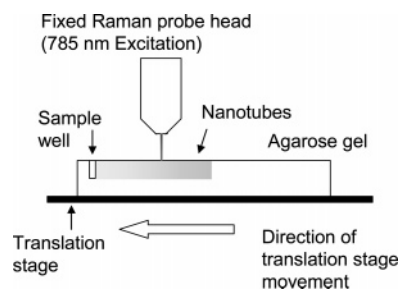

Figure 3. Diagram of the apparatus used for Raman/fluorescence spectroscopy on agarose gels. The gel sits on a translation stage which moves 0.5 mm between spectra taken through a probe head in which excitation and emission light use the same aperture.

peaks and one fluorescence peak plotted versus distance from the sample wells. The maximum of each feature occurs at different distances. The 213 cm^{-1} (9,7) ($d = 1.103$ nm) feature reaches its maximum intensity at approximately 64.5 mm into the gel. The 231 cm^{-1} (12,1) ($d = 0.995$) RBM reaches its maximum at 61.5 mm from the well. These preferential migrations occur only for nanotubes exposed to extended probe-tip sonication. Figure 4b shows migration of material subjected to cuphorn sonication for 10 min only.

In a gel containing material sonicated for 10 h, a Raman spectrum at 71.5 mm from the sample wells shows the (9,7) and (12,1) features at approximately equal intensity (Figure 4e). The high relative intensity of the (9,7) RBM, normally diminutive in a HiPco sample, implies enrichment of the large (9,7) nanotube at this position in the gel.[30] Conversely, a Raman spectrum at 45 mm from the origin shows only the smaller (12,1)

(29) Burghard, M.; Duesberg, G.; Philipp, G.; Muster, J.; Roth, S. *Adv. Mater.* **1998**, *10*, 584–588.
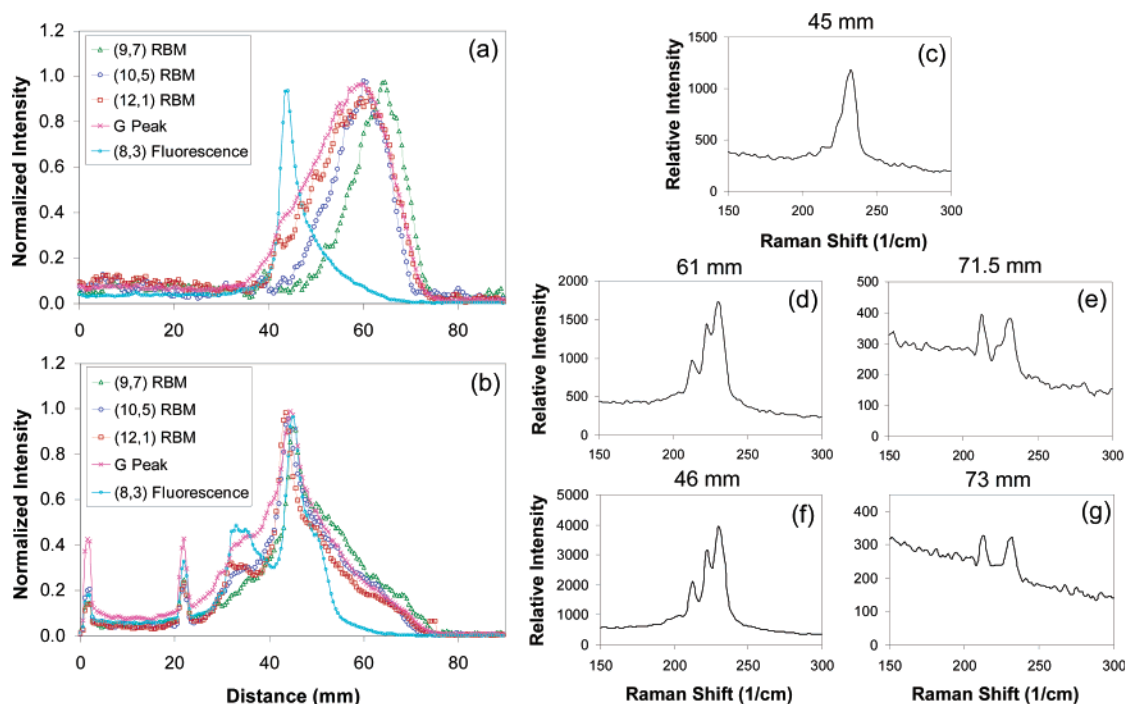
Figure 4. Profiles of five Raman and fluorescence nanotube features and selected Raman RBM spectra in an agarose gel run for 1 h with a 100 V applied potential. Peak heights are recorded versus distance from the sample well. Profiles are normalized with respect to the maximum height of each feature. (a) Profile of nanotubes probe-tip sonicated for 10 h. (b) Profile of nanotubes probe-tip sonicated for 0 h. (c−e) Spectra of Raman RBM regions of nanotubes probe-tip sonicated for 10 h, taken (c) 45 mm, (d) 61 mm, and (e) 71.5 mm from the sample wells. (f−g) RBM spectra of nanotubes probe-tip sonicated for 0 h taken (f) 46 mm and (g) 73 mm from the sample wells. (A spectrum analogous to (c) was not found.)

RBM, implying this species' slower average movement through the agarose gel (Figure 4c). The 223 cm^{-1} RBM, corresponding to the (10,5) nanotube ($d = 1.050$ nm), reaches its maximum at the same location as the (12,1) feature, though in all samples of intermediate sonication times (1−5 h), the peak appears to migrate faster than the (12,1) RBM and more slowly than the (9,7) RBM, consistent with other observations of diameter-dependent Raman peak migration.[8] Analogous RBM changes are found in Raman spectra taken at 633 nm excitation (Supporting Information). The effect is apparently independent of the surfactant used. Nanotubes suspended and sonicated in sodium dodecyl sulfate (SDS) show relative changes in the RBMs similar to those of sodium cholate-suspended tubes if electrophoresed with sodium cholate or Triton X-100 surfactant in the running buffer. We note, however, that, if SDS is used in a running buffer, nanotubes flocculate in the gel.

In the agarose gels, electrophoretic mobility, $\mu = q/f$, depends on the molecular charge, q, and on the frictional coefficient, f, which is dependent on the solution viscosity and the molecular size of the analyte. To elucidate the cause of the mobility increase, size exclusion chromatography was used, as this technique separates species solely by molecular size. A sample sonicated for 3 h was run through a 100 cm size exclusion column (i.d. = 1.5 cm) using a high-resolution gel filtration medium composed of allyl dextran and *N,N′*-methylenebis-acrylamide. The eluate was fed by a peristaltic pump at 0.5 mL/min through absorption and Raman spectrometers to record a UV−vis−near-IR spectrum every 4 min and a 785 nm Raman spectrum every 30 s (Figure 5a). Raman and fluorescence profiles of peak intensity versus elution time in the column

(Figure 5b) show behavior qualitatively similar to that of the Raman and fluorescence profiles for electrophoresed nanotubes sonicated for 3 h (Figure 5c). All nanotube species elute in the same order using both gel electrophoresis and size exclusion chromatography, and analogous RBM spectra are found in both techniques (provided in the Supporting Information). We therefore conclude that the distinct electrophoretic mobilities of nanotubes result from molecular size differences only. Since length contributes to the vast majority of size differences in nanotubes, the mobility is deemed largely length dependent.
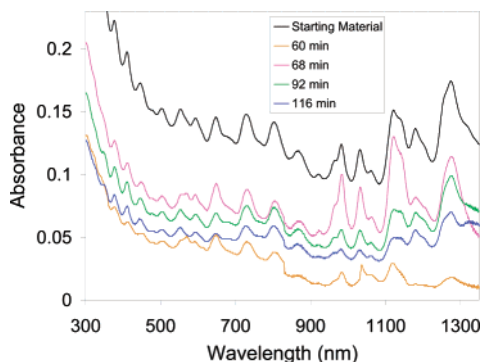
Absorption spectra of the size exclusion column-separated nanotubes show that the diameter distribution of nanotubes changes across fractions (Figure 6). Focusing on the E$_{11}$ transition peaks (900 nm and higher), we note that transition wavelength is roughly monotonic with respect to diameter in this region. Using this assumption, we see that the fraction eluted at 60 min is enriched in small-diameter nanotubes when compared to the starting material. However, during elution, the long-wavelength peaks at 1280 and 1185 nm increase with a concomitant decrease in the short-wavelength peaks at 980, 1036, and 1130 nm. This implies a change in the diameter distribution with elution time. Absorption spectra of nanotubes electroeluted from agarose gels show behavior analogous to that of absorption spectra of column-separated nanotubes (provided in the Supporting Information). In the E$_{11}$ region again, short-wavelength peaks appear in early fractions, followed by longer wavelength peaks in later fractions. Absorption spectra therefore supplement the argument for diameter separation.

Changes in nanotube optical spectra have been correlated to various phenomena other than selective enrichment or depletion of certain species.[31,32] For example, bundling (aggregation) of nanotubes changes the Raman resonances due to electronic

---

(30) We reject the possibility of aggregation causing spectral changes here because nanotube fluorescence disappears during aggregation.
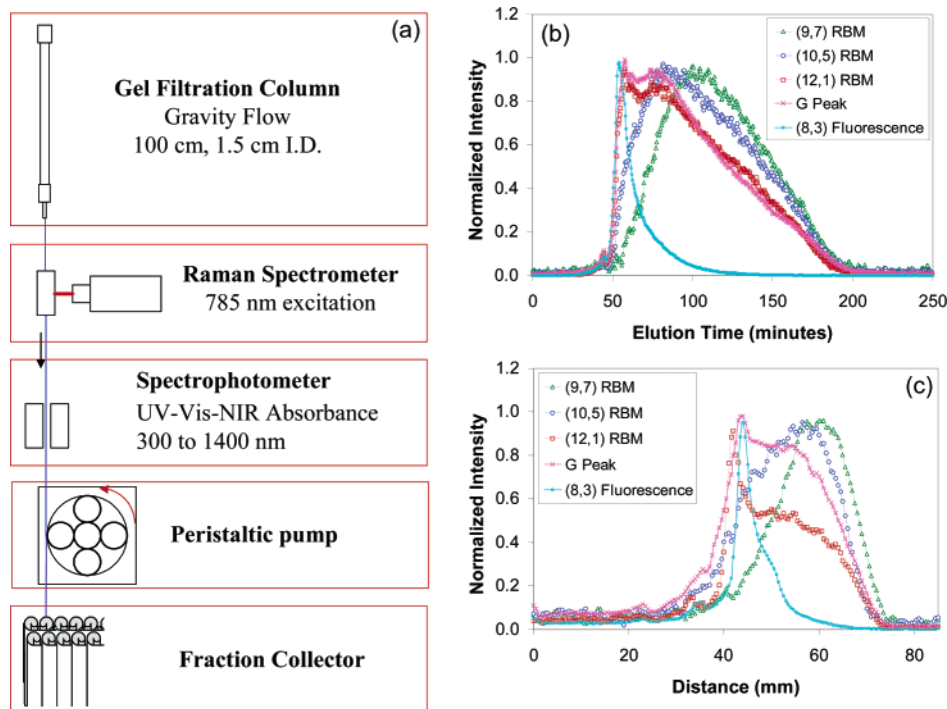
Figure 5. (a) Diagram of the size exclusion chromatography experiment. A 100 cm gravity flow column elutes into a tube connected to a Raman spectrometer and a UV−vis−near-IR spectrophotometer. A peristaltic pump draws the eluate through the apparatuses and into a fraction collector. (b) Profile of five Raman and fluorescence peaks during a size exclusion chromatography experiment using nanotubes probe-tip sonicated for 3 h. (c) Profile of an agarose gel containing nanotubes probe-tip sonicated for 3 h run at previous conditions. Profiles were normalized with respect to the maximum height of each feature.

Figure 6. Absorption spectra of selected fractions of nanotubes probe-tip sonicated for 3 h and separated by a size exclusion column. The spectra show changes in the concentrations of the nanotube species with respect to elution time.

dispersion between tubes in contact with each other.[31] By corroborating Raman changes with absorption and fluorescence spectroscopies, however, this possibility can be eliminated. Fluorescence spectra of electroeluted fractions taken from 900 to 1400 nm emission are compared to absorption and Raman spectra (Figure 7). At 650 nm excitation, fluorescence shows changes analogous to those of the absorption spectra. The large-diameter nanotubes (9,7), (10,3), and (8,6) appear in the first electroeluted fraction, F1. It should be noted that the (9,7) and (10,6) features are off-resonance at 650 nm, though they appear at an intensity equal to or greater than that of the other peaks in the spectrum. The spectrum of F5 shows that the three large-diameter peaks are absent or dwarfed by the smaller diameter nanotube features, (8,3), (7,5), and (7,6).

Raman, absorption, and fluorescence spectra of gel and column fractions all suggest that nanotube species of larger diameters move in unison with small molecular sizes. Separation by diameter is thus concomitant with length fractionation, and nanotubes that have been cut shortest also possess the greatest relative enrichments of large-diameter species. As longer sonication time causes increased electrophoretic mobilities in the gels, we credit sonication for determining the degree of both length and diameter separation of the nanotubes.

Mechanism and Implications of Diameter Separation. We assert that selective depletion and enrichment of certain nanotube species have occurred in our fractions, though changes in optical properties of carbon nanotubes with length fractionation could arguably be attributed to various length-dependent optical effects.[33] For instance, Rochefort et al. predicts an increase in metallic nanotube band gap with decreasing nanotube length using ab initio and semiempirical calculations on zigzag ($n = m$) nanotubes. According to Rochefort, finite-length effects do not change the band gap until nanotubes are 5−10 nm in length, corresponding to the 1-D to 0-D transition. Scanning tunneling microscopy experiments show that band gap changes occur when nanotubes are cut to a few tens of nanometers.[34] Therefore, it is unlikely that we are seeing these particular finite-length effects in our nanotubes.

All fluorescence features measured in the agarose gel (Figures 4 and 5) migrate approximately 44−45 mm into the gel, though RBM maxima elute approximately 20 mm farther down the lane. Five fluorescence features are measured (corresponding to the (8,3), (6,5), (7,5), (6,4), and (9,1) nanotubes), and all curves

(31) Heller, D. A.; Barone, P. W.; Swanson, J. P.; Mayrhofer, R. M.; Strano, M. S. *J. Phys. Chem. B* **2004**, *108*, 6905−6909.
(32) Baik, S.; Usrey, M. L.; Rotkina, L.; Strano, M. S. *J. Phys. Chem. B* **2004**.
(33) Rochefort, A.; Salahub, D. R.; Avouris, P. *J. Phys. Chem. B* **1999**, *103*, 641−646.
(34) Venema, L. C.; Wildoer, J. W. G.; Janssen, J. W.; Tans, S. J.; Tuinstra, H. L. J. T.; Kouwenhoven, L. P.; Dekker, C. *Science* **1999**, *283*, 52−55.
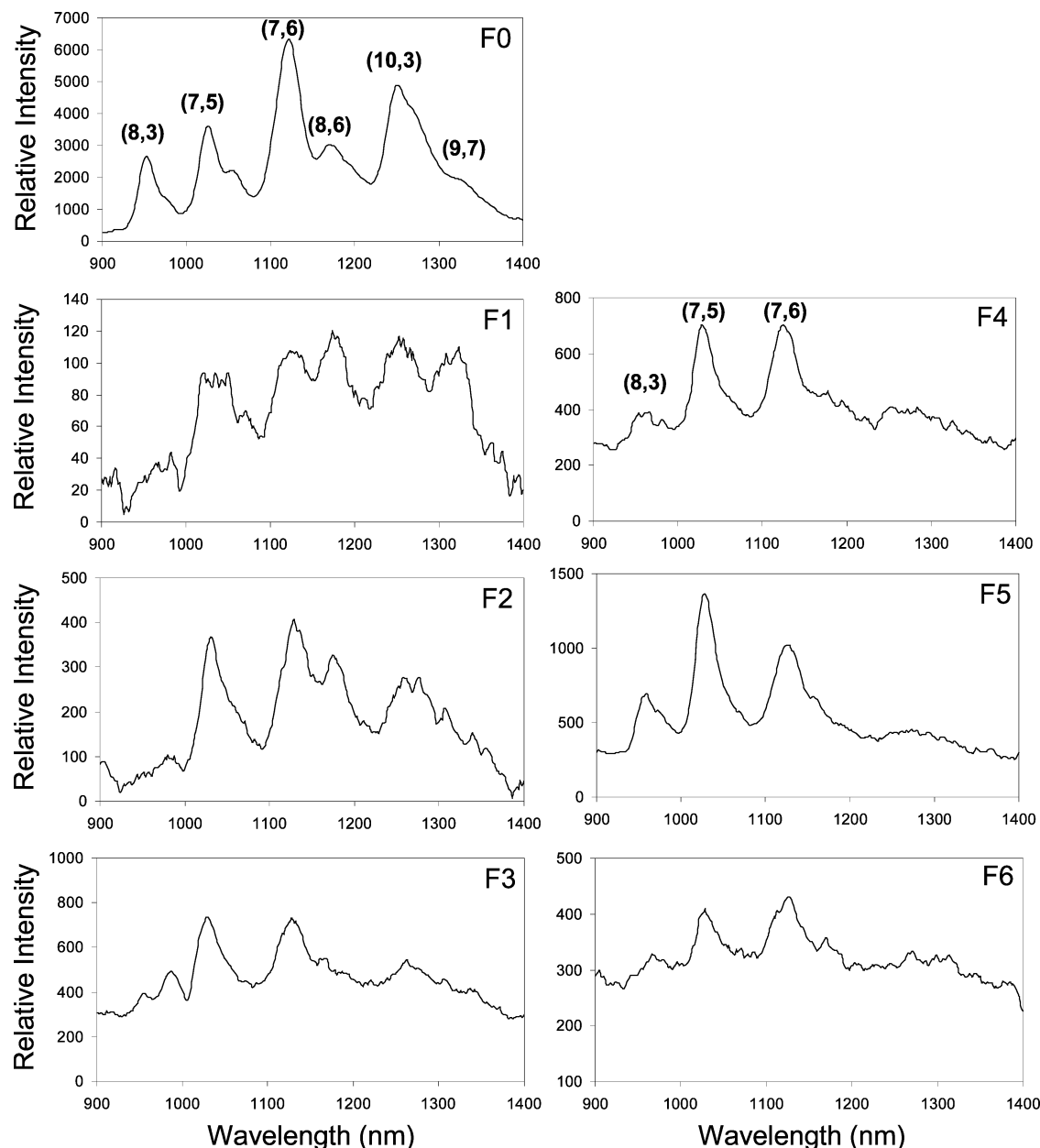
Figure 7. Near-infrared fluorescence spectra of the six fractions electroeluted from an agarose gel and the starting material, taken at 650 nm excitation.

exhibit similar shapes. For clarity, only the (8,3) peak is shown as all fluorescence features exhibit approximately the same behavior as the (8,3) peak. Fluorescence features measured by this method correspond to smaller diameter nanotubes than those appearing in the Raman spectra, potentially explaining the early maxima relative to the RBMs (i.e., these small-diameter nanotubes are disproportionately longer). However, the early maxima and subsequent intensity decrease with the tube lengths in the gels, and the column could also signify a decrease in quantum yield with the shortening of nanotubes.

A rough method of calculating relative quantum yields of nanotubes of different lengths was employed for the six fractions electroeluted from an agarose gel. The relative quantum yield is estimated using $\Phi_r = F_{\text{feature}}/A_{\text{feature}}$, where A_{feature} and F_{feature} are the absorbance and fluorescence intensity of the sample at the center wavelength of a particular nanotube transition. Due to the convoluted nature of the absorption spectrum, this is inexact. The relative quantum yields of the fractions are

calculated using an absorption peak at 1036 nm and a fluorescence peak at 1028.50 nm, corresponding to the (7,5) nanotube, as well as an absorption feature at 1125 nm and fluorescence at 1122.88 nm, consistent with the (7,6) nanotube. In both cases, the quantum yield is found to increase exponentially with respect to the average nanotube length (measured via AFM) (Figure 8).

Our diameter-selective cutting results run counterintuitive to certain chemical and mechanical arguments. Sonication is believed to cut nanotubes because collapsing cavitation bubbles create localized areas of high pressure and temperature in the vicinity of the nanotube sidewall. Continuum mechanics arguments are used to model this cutting process. Shear and normal forces are calculated on a hypothetical hollow cylinder.[35] Normal stresses are determined by

$$\sigma = \frac{M}{\pi r^2 t} \tag{1}$$
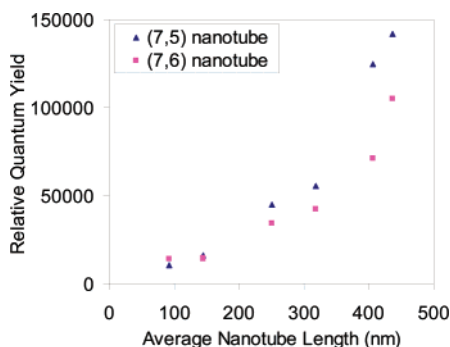
Figure 8. Relative quantum yields of the (7,5) and (7,6) nanotubes, electroeluted from an agarose gel, plotted versus average nanotube length as measured by AFM.

where M is the bending moment on a cylinder, t is the thickness of the wall (held constant), and r is the average of outer and inner radii. Shear stresses are modeled using

$$\tau_{\max} = \frac{4V}{3A} \frac{3r^2 + 3rt + t^2}{4r^3t + 6r^2t^2 + 4rt^3 + t^4} \qquad (2)$$

where V is the shear force acting on a cross section and A is the cross sectional area, $\pi(r_2^2 - r_1^2)$.

Relative shear and normal forces calculated for the nanotubes measured by Raman spectroscopy predict the cutting behavior opposite that observed spectroscopically, as the calculated stresses decrease with increasing nanotube diameter. Also in disagreement with our separation results are the pyramidalization and π-orbital misalignment angles.[36] Both are inversely proportional to nanotube diameters and directly proportional to predicted reactivities of nanotube species. Smaller diameters, according to these indicators, should lead to decreasing stability and shorter nanotubes. Therefore, strain caused by pyramidalization or π-orbital misalignment cannot explain SWNT cutting by sonication.

Zhang and Iijima report that the larger diameter SWNTs prepared by laser ablation contain more defects than smaller diameter SWNTs.[37] Similar behavior during the HiPco process could explain preferential cutting of nanotubes during sonication, as nanotubes weakened by defects are more easily cut. Alternatively, Miyauchi et al. illustrates the unusual stability imparted to some small-diameter nanotubes by end caps which follow the isolated pentagon rule, used to describe stable fullerene structures.[38] Experiments designed to elucidate the mechanism of diameter-dependent cutting are in progress.

Conclusions

Gel electrophoresis and column chromatography conducted on ultrasonicated single-walled carbon nanotubes yield concomitant separation of tube lengths and diameters. These scalable processes generate nanotube fractions with narrow length distributions and altered diameter populations. The cutting process is diameter selective, and the distribution of nanotubes changes with sonication time. The ability to control this distribution will permit nanotubes to be isolated by diameter in preparative quantities. Development of nanotube-based applications will require the manipulation of nanotube lengths and diameters described herein.

Supporting Information Available: Raman spectra of material processed by size exclusion chromatography and Raman and absorption spectra of electroeluted gel fractions (PDF). This material is available free of charge via the Internet at http://pubs.acs.org.

JA046450Z

(35) Gere, J. M.; Timoshenko, S. P. *Mechanics of Materials*, 3rd ed.; PWS-Kent: Boston, 1990.
(36) Niyogi, S.; Hamon, M. A.; Hu, H.; Zhao, B.; Bhowmik, P.; Sen, R.; Itkis, M. E.; Haddon, R. C. *Acc. Chem. Res.* **2002**, *35*, 1105−1113.
(37) Zhang, Y.; Iijima, S. *Philos. Mag. Lett.* **1998**, *78*, 139−144.
(38) Miyauchi, Y. H.; Chiashi, S. H.; Murakami, Y.; Hayashida, Y.; Maruyama, S. *Chem. Phys. Lett.* **2004**, *387*, 198−203.